Available online at www.sciencedirect.com
SCIENCE DIRECT®
ELSEVIER
Palaeogeography, Palaeoclimatology, Palaeoecology 235 (2006) 288–304
PALAEO
www.elsevier.com/locate/palaeo

Insolation-control on the Late Cretaceous hydrological cycle and tropical African climate—global climate modelling linked to marine climate records

Sascha Floegel [a,*], Thomas Wagner [b]

[a] *IFM-GEOMAR Leibniz-Institute of Marine Sciences, Wischhofstr. 1-3, 24148 Kiel, Germany*
[b] *School of Civil Engineering and Geosciences, University of Newcastle, Newcastle upon Tyne, NE1 7RU, UK*

Accepted 12 September 2005

Abstract

Data from Late Cretaceous paleoclimate simulations and their linkage to a geological model derived from long-term high-resolution proxy-data indicate and support strong relationships between African climate and tropical Atlantic sedimentation. Here, we present results from an interdisciplinary study.

By varying only one parameter in the set of orbital boundary conditions of the numeric model, we focus on the climatic impact of precessional forcing on the global and regional climate system. As a result, new insights to the internal dynamics of climate, the different compartments and fluxes of the hydrological cycle, and finally the sedimentary response within the oceanic realm during greenhouse conditions have been approached. The climate models suggest that insolation changes at 25–55°S are the trigger for cyclic variations of the tropical hydrological cycle of northern Africa. Between the various models, a maximum difference in insolation at the top of the atmosphere of 14 W/m^2 is needed to produce the documented changes in the hydrological cycle. First of all, the simulations do not suggest any substantial latitudinal movement of the ITCZ over the course of one precessional cycle. The models rather indicate cross-latitudinal variation of pressure systems and variation in the magnitude and direction of surface winds, linking tropical Africa to the mid-southern latitudes. This cross-latitudinal atmospheric teleconnection denotes a reduced role of the tropics as driver of Cretaceous climate system. Therefore, the linkage of proxy-based geological and numeric models rather supports the idea that tropical Atlantic black shale formation in the Late Cretaceous was ultimately triggered by climate change in mid-southern latitudes, with precipitation and river discharge being the transport mechanisms.

As a hypothesis that will be tested in the near future, we speculate that the mid-latitudes represent the "ultimate" region of climate signal formation during times of extreme global warmth.

Keywords: Paleoclimate; Cretaceous; Hydrological cycle; Latitudinal atmospheric connection; Marine geochemical signal formation; Black shale formation

1. Introduction

A surge of high-quality marine and continental paleoclimate records has become available in recent years that stimulated integrated research on climate and ocean dynamics during periods of extreme warmth,

* Corresponding author. Fax: +49 413 600 2941.
E-mail address: sfloegel@ifm-geomar.de (S. Floegel).

0031-0182/$ - see front matter © 2005 Elsevier B.V. All rights reserved.
doi:10.1016/j.palaeo.2005.09.034

e.g., the mid-Cretaceous (Huber, 1998; Poulsen et al., 2001; Wilson and Norris, 2001; Voigt et al., 2004). These new proxy records have provided a more precise picture of how atmospheric and ocean properties have changed in response to climate fluctuations and orbital forcing. One of the major challenges in Cretaceous research remains: the deficiency to properly link and validate the geological record with computer-based climate models. This partially occurring model-data discrepancy limits the ability to predict the effects, e.g., of continental topography, vegetation and hydrological cycling on ocean properties and, ultimately, marine sedimentation. While progress in proxy research is challenged by model-data discrepancies, it is also well positioned to evaluate the reliability and robustness of computer-based models commonly used for future climate prediction. This study provides an example from the Late Cretaceous Coniacian–Santonian where implications from high-resolution climate records of Eastern Equatorial Atlantic ODP Site 959 (Wagner and Pletsch, 1999; Pletsch et al., 2001; Wagner, 2002) are validated and further developed using new results from global climate modelling.

The geological model is based on Late Coniacian–Early Campanian millennial-scale marine and continental proxy records from ODP Site 959. They reveal a pronounced and persistent cyclicity that was attributed to orbital-forced (mainly precessional) fluctuations in continental supply from different African source areas and deep water redox conditions during the main period of the Oceanic Anoxic Event 3, the OAE-3 (Hofmann et al., 2003). These repetitive fluctuations in atmospheric and oceanic properties drove drastic changes in the rate of organic carbon burial (Beckmann et al., 2005a) and were accompanied by extreme open ocean redox conditions, i.e., the temporal establishment of photic zone euxinia (Wagner et al., 2004). The estimated average transient times from oxygenated to oxygen-depleted environmental conditions off Equatorial Africa were short, on the order of a thousand years or less; the duration of peak organic carbon supply and thus black shale formation was remarkably constant at about 5000 years followed by a gradual recovery period of about the same duration (Beckmann et al., 2005a). The precise onset and offset of peak organic carbon burial and its total duration of about 5000 years apparently was controlled by precessional forcing. The onset of maximum organic carbon burial rates, however, was delayed by about 1000 years relative to the runoff from tropical Africa (Fig. 1, Beckmann et al., 2005a) supporting the conclusion that ocean properties in the tropical Late Cretaceous Atlantic reacted to rather than triggered atmospheric circulation and hydrologic cycling. Simulation of total continental runoff from tropical Africa between 1–19°S and 15–45°W has shown that a pre-

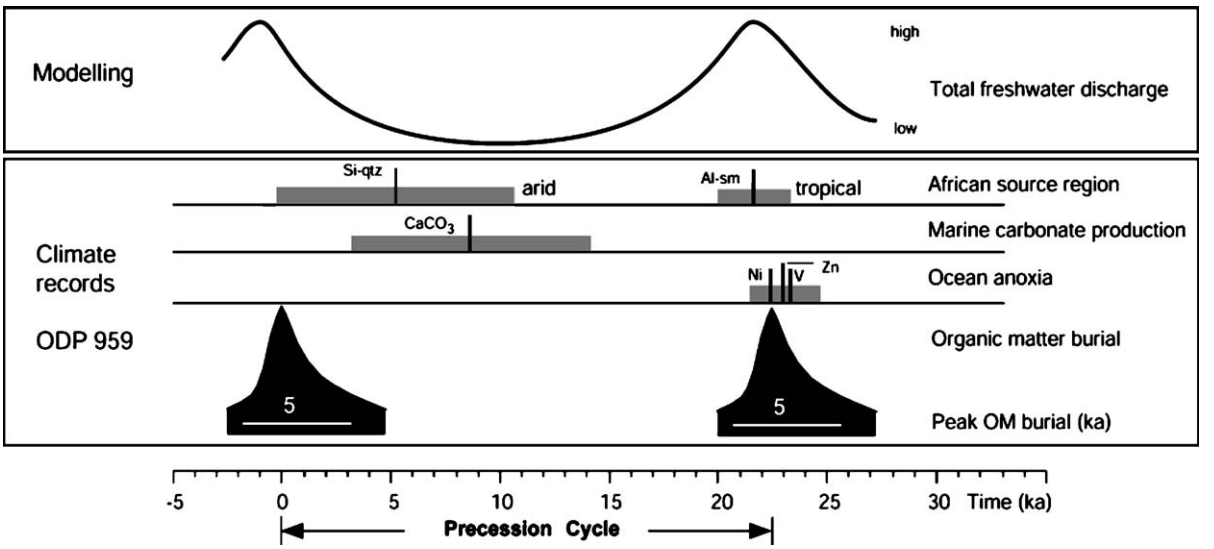

Fig. 1. Idealized, average precession cycle at ODP Site 959 with approximate transition times (ka) for the onset and decay of peak OC accumulation, i.e. the change from background to black shale depositional modes (modified from Beckmann et al., 2005a) in relation to simulated continental runoff. The timing of peak accumulation of parameters indicative of carbonate productivity ($CaCO_3$), redox conditions (Ni, V, Zn), input from arid source regions (silicium, attributed to quartz deposition, "Si-qtz") and tropical source areas (aluminium, attributed to smectite deposition "Al-sm") in respect to peak OC accumulation are shown according to Beckmann et al. (2005a). Solid lines mark average peak values; shaded bars indicate standard deviation of each individual proxy (Beckmann et al., 2005a).

cessional angle of 90° of the northern winter solstice (equivalent to modern spring configuration in an annual orbital cycle) caused the most extreme climatic contrasts on Africa, which promoted black shale deposition for the length of one-quarter of a precessional cycle, i.e., about 5000 years (Beckmann et al., 2005b).

The climate record-based geological model implies some principle relationships between African climate and tropical Atlantic sedimentation that raise a number of fundamental questions. Where was the climate trigger located, in the tropics or at higher latitudes? If at higher latitudes what mechanisms connected the trigger source area to the response area? The nature of these questions is fundamental to verify the climate record-derived model and requests an approach that provides and links different critical climate parameters at local, regional and global scale. Global climate modelling is capable of providing and integrating these data, and thus has the capacity to improve models from geological records.

We performed numerical simulations using the GENESIS (*G*lobal *En*vironmental *E*cological *S*imulation of *I*nteractive *S*ystems) General Circulation Model 2.0. Due to its design, GENESIS 2.0 is able to allow investigation of the effect of precession of the equinoxes on the hydrological cycle by assessing global air temperature and pressure, wind fields, precipitation and surface and subsurface runoff, and ultimately total river discharge. Different from previous modelling approaches, this study specifically examines the influence of precessional changes through intermediate setups allowing the analysis of one complete cycle as a continuum passing all of its four end member constellations, i.e., summer, spring, autumn and winter (in this study referred to as orbital cases A through D).

2. Methods

2.1. The GENESIS atmospheric general circulation model

The general features of the GENESIS Earth System Model, designed for paleoclimate research, have been presented in Pollard and Thompson (1995), Thompson and Pollard (1995, 1997) and Covey and Thompson (1989). Some specific features of GENESIS are the use of an *A*tmospheric *G*eneral *C*irculation *M*odel (AGCM) as its core component, which is coupled to a 50 m mixed slab ocean model and multilayer models of soil, snow and sea ice. Resolution of the AGCM is $3.75° \times 3.75°$ and that of the Land Surface Transfer Scheme (LSX) is $2° \times 2°$.

2.2. Boundary conditions

Boundary conditions were set for the early Late Cretaceous (93 Ma, earliest Turonian). The modelling approach to use a 93 Ma paleogeography and the according boundary conditions for geological proxy data from about 85 Ma (Coniacian) is based on the assumption that geography as well as atmospheric boundary conditions did not change too much to justify a new set of boundary conditions. Based on our present knowledge on the climate system of the Late Cretaceous, the presented modelling framework is applicable to both time slices. Forcing factors and paleogeography were set as follows: the solar constant was specified to be 98.62% (1337.0 W/m^2) of the present value of 1365.0 W/m^2. It is based on estimates of solar luminosity calculated from a standard model of solar evolution (Gough, 1981). Heat transport in the slab ocean model was prescribed with values similar to those of today. Atmospheric CO_2 was specified as 1881.6 ppm, which is about 6× the pre-industrial level of 313.6 ppm and about 5× the present value of 365 ppm. This value is in the middle of the range of estimated values of 1.5 and 9 times present for the Late Cretaceous (DeConto et al., 2000). Berner (1994, GEOCARB II) estimated the CO_2-values to be between 1.5 and 5 times present, based on a long-term geochemical carbon cycle model. Cerling (1991) calculated a Barremian to mid-Albian (Early Cretaceous) atmospheric CO_2 of 1500–3000 ppm, or about 4.4–9 times present, from the carbon isotopic composition of soil carbonate in paleosols. Concentrations of atmospheric CH_4 and N_2O were set at pre-industrial levels, 0.800 ppm and 0.288 ppm, respectively. The vegetation type used for this model is "Type 6" (broadleaf trees with groundcover—savanna) after Dorman and Sellers (1989), and assumed to cover all land areas. The soil model used for these simulations is a globally uniform module, consisting of 51% sand, 29% silt and 20% clay, which is a simplification to reduce run duration of the models.

The land–sea distribution was obtained from global paleogeographic reconstructions of Balukhovsky et al. (2004). Their map is based on two Atlases of "Lithological-Paleogeographic Maps of the World" that contain data on the lithological composition and thicknesses of sediments and volcanics formed during 28 different intervals of the Paleozoic (Ronov et al., 1984) and Mesozoic–Cenozoic (Ronov et al., 1989). The data on sediment distribution and volumes are presented in the context of the paleogeographical environments and tectonic regimes, which governed sediment deposition. The paleogeography, terrestrial

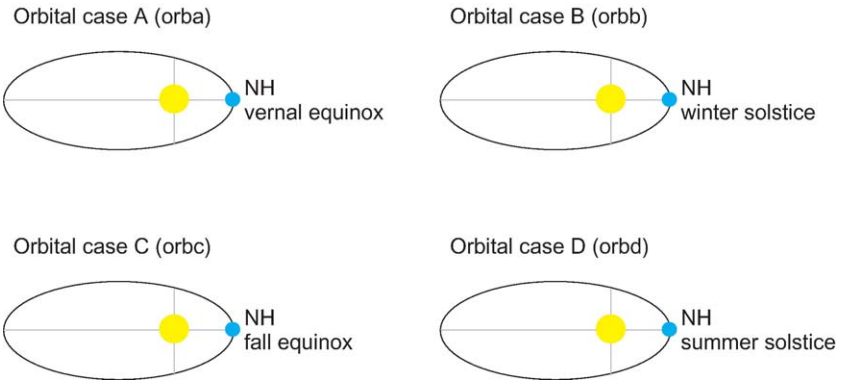

Fig. 2. Orbital boundary conditions for one complete precessional cycle (after Floegel et al., 2005).

elevations and vegetation were than interpolated to $2^\circ \times 2^\circ$ resolution.

2.3. Model simulations

Five experiments (1 control run + 4 orbital runs with changing precession) were carried out for this study (Fig. 2). Previous simulations of the Cretaceous climate system changed all three orbital parameters (eccentricity, obliquity and precession) to explore the effect of differences between total maximum and minimum forcing ("hot summer orbit/cold summer orbit approach"; Crowley et al., 1993; Sloan and Morrill, 1998). To assess and quantify the individual effect of precessional forcing, we changed only the precession of the equinoxes as a parameter for each run. Eccentricity was fixed during all orbital runs at a value of 0.05 because it allows for maximum seasonality. Obliquity was fixed at the present value of 23.5°.

The "control run (cold)" used in this study has an eccentricity of 0.00, which eliminates any precessional effects. The result is a circular orbit of the earth around the sun. Seasonal precession has therefore no climatological effect (precess. = ecc. * sin ϖ). In GENESIS, precession is defined as the prograde angle from perihelion to the vernal equinox. It differs from some other definitions by multiples of 90° (Table 1). All orbital parameters were defined within a range of orbital values given by Berger (1978).

2.4. Model sensitivity and validation

Global paleoclimate modes such as GENESIS 2.0 are not specifically designed to simulate regional precipitation and discharge patterns, and seasonality for small geographic areas with large precision. We therefore compare simulated precipitation data from GENESIS for modern NW-Africa between 9–19°N and 9°W–9°E to measured and modelled data from the literature to validate the quality of the simulated data. Modern annual precipitation for the region of 10–20°N/10°W–10°E is measured to be 638 mm/year[5]. GENESIS 2.0 provides modern annual precipitation values of 642 mm/day at 2 m height above surface (D. Pollard, unpublished data), which are above the 95% confidence level of the predicted values provided by satellite measurements (http://www.cpc.ncep.noaa.gov/products/african_desk/meteosat/) testifying to the quality and significance of GENESIS

Table 1
Orbital parameters for control (cold) run and simulations with varying precession of the equinoxes (orbital runs)

	Precession	Perihelion	Climatic effect
Control run (cold)	–/– (eccentricity = 0.0)	–/–	–Circular orbit of the earth around the sun –No seasons
Orbital case A (orba)	0/360	Spring equinox, March 21	–Spring warmer than normal (northern hem.) –'Intermediate forcing' for winter and summer months
Orbital case B (orbb)	90	Winter solstice, December 21	–Warmer than average winter (northern hem.) –Colder than average summer (northern hem.)
Orbital case C (orbc)	180	Fall equinox, September 21	–Fall warmer than normal (northern hem.) –'Intermediate forcing' for winter and summer Months
Orbital case D (orbd)	270	Summer solstice, June 21	–Summer warmer than average (northern hem.) –Winter colder than average (northern hem.)

2.0-derived modelling data. Because the chosen area of tropical N-Africa is highly sensitive to precipitation, it is situated on the border between the ITCZ to the south and the very dry Saharan subtropics to the North, we analyzed the global and regional performance of GENESIS to simulate present day seasonality in the tropics. Comparison of global monthly mean precipitation for January and July reveals a striking match between the simulated and observed (Shea, 1986) records (Fig. 3) confirming the quality of GENESIS to simulate modern seasonal pattern on a global scale. Precipitation values for the tropical African study area are 0.0023/3.76 and 0.071/4.69 mm/day for January/July for the chosen rectangle for GENESIS and observed, respectively. Considering the sensitive location and the large seasonal variation of the study area, the agreement between simulated and observed data is very good.

3. Results

3.1. Global patterns of a greenhouse hydrological cycle

Monthly modelling results of continental total river discharge reveal a pronounced wet season from March to June with total discharge accounting for 56% to 71% of the total annual discharge (Beckmann et al., 2005b) and a dry season from July to February (Fig. 1). Maximum river discharge occurred during April and May approaching maximum values of 3.58 mm/day for orbital case A. Strongest seasonal contrasts occurred during orbital case A, whereas smallest contrasts are indicated for orbital case C suggesting most equilibrate climate conditions. In order to evaluate how changes in total discharge relate to precessional forcing and thus orbital configuration we analyze global patterns of key parameters defining Earth's climate system and the hydrological cycle for the month of March, i.e., air temperature, air pressure at sea level, surface winds and precipitation.

3.1.1. Air temperature at surface

Air temperature is one key climate parameter, being directly influenced by orbitally driven changes in insolation. For the month of March, the control run simulation suggests a global meridional temperature gradient of about 30–35 °C (Fig. 4A), ranging from ~30 °C in the tropics to ~0 °C to −5 °C in both polar regions. Between 30°S–15°N, air temperatures approach about 28–30 °C, with the continental interiors heating up to 35–37 °C. At intermediate latitudes from 30°S to 45°S and 15°N to 30°N, air temperatures vary between 18 and 25 °C. They further decrease to 15 °C to −5 °C

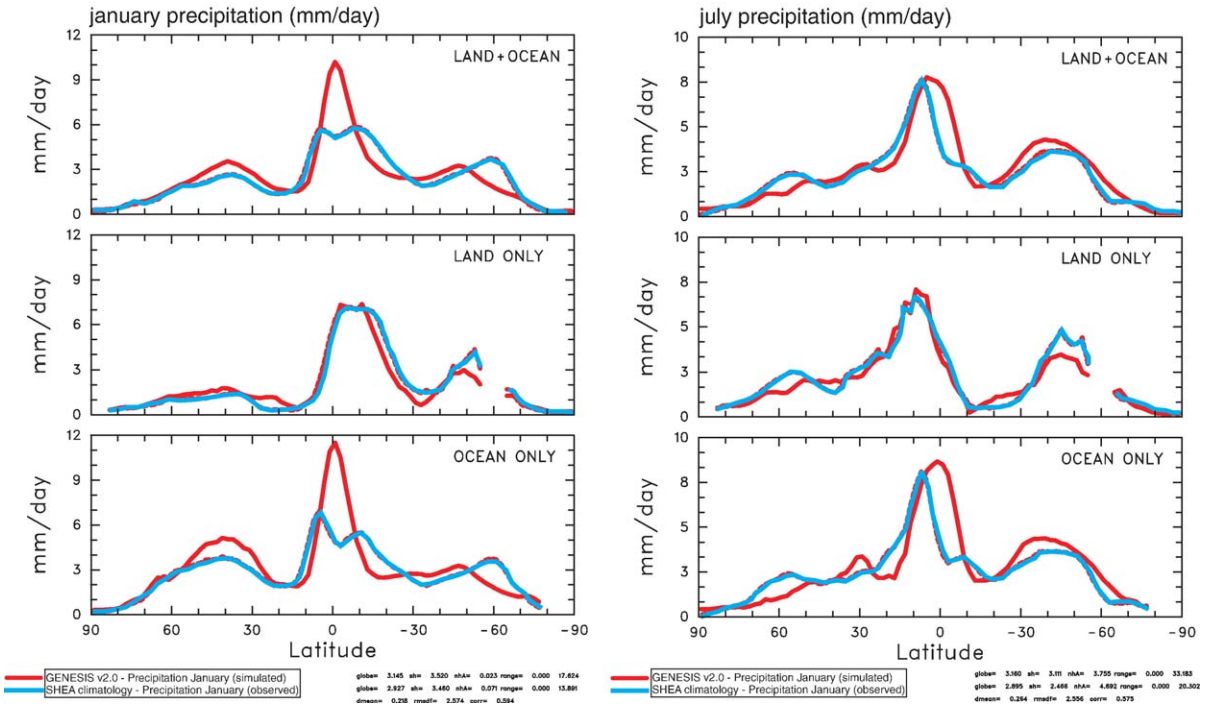

Fig. 3. Comparison of global monthly mean precipitation for January and July. Simulated (GENESIS v2.0—red curve) and observed (Shea, 1986—light blue curve). (For interpretation of the references to colour in this figure legend, the reader is referred to the web version of this article.)

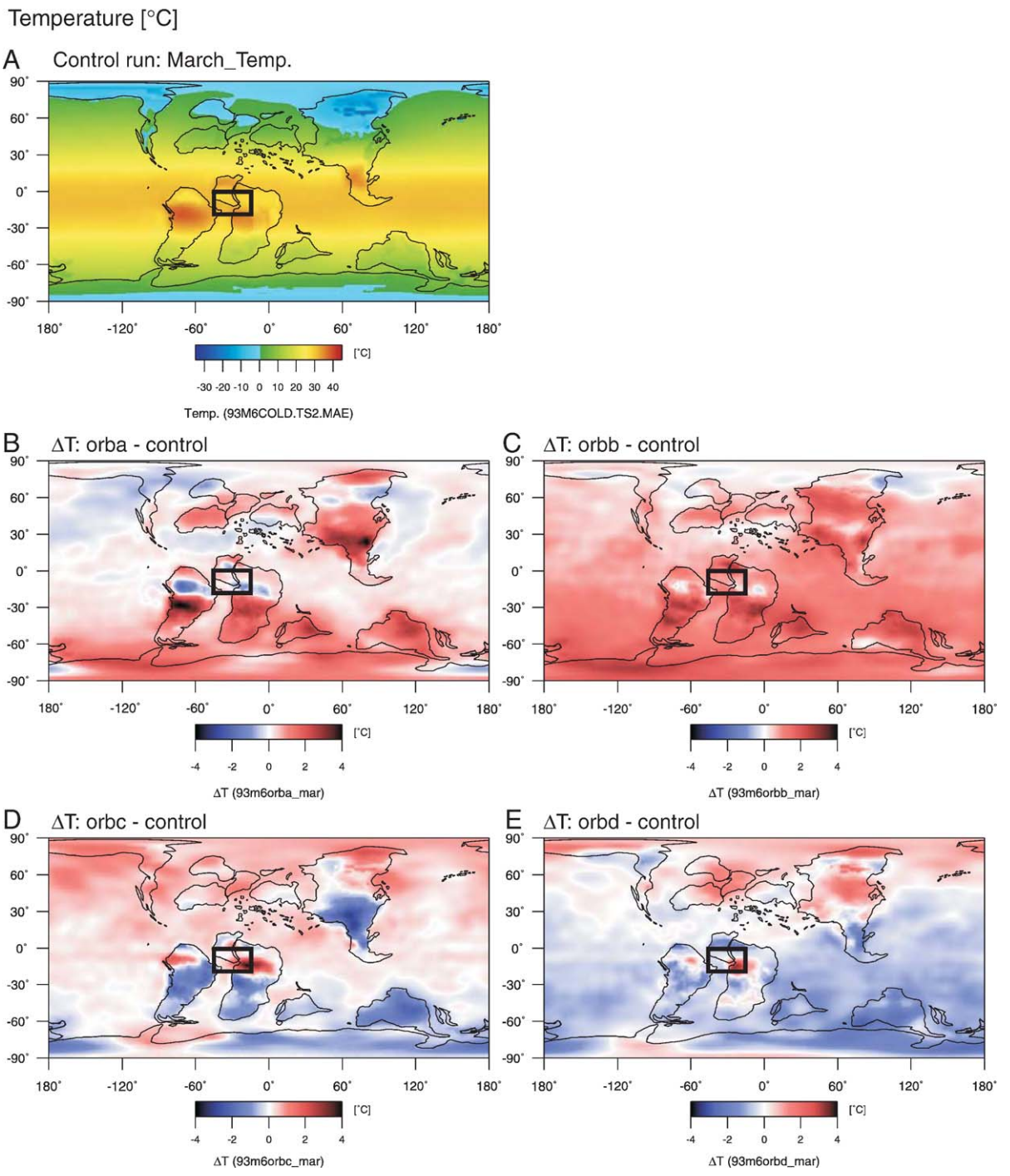

Fig. 4. Distribution of air temperature at 2 m heights (°C) for the month of March for control run (A) and orbital (B–E) runs. As for the consecutive figures, the control run defines reference conditions and the rectangle in tropical Africa represents the area considered for regional budget calculations. Simulation results from the precession experiments are displayed as difference to the reference conditions (control run).

at high latitudes between 45–90°S and 30–90°N. Lowest values are simulated for central Antarctica and the high northern latitudes between ~75° and 90°. Exceptions are the extremely cold continental interiors of Asia (down to −24 °C) and the mountainous regions of western North America (about −10 °C at 45°N). These low temperatures over the continental interiors are possibly due to the missing interactive vegetation

in the setup of GENESIS. The prescribed fixed vegetation, savanna, does not provide high latitude forests, which are needed to maintain polar warmth and equable continental interiors (DeConto et al., 2000), whereas the low temperatures over the Sevier Highlands of western North America are affected by the high altitudes (up to 3000 m) proposed for that region (Floegel et al., 2005). Air temperatures of 25–30 °C are simulated for the tropical African study area between 1–19°S and 15–45°W.

The four orbital runs (Fig. 4B–E) show a continuum of air temperature variation with changing orbital precession. The largest deviations relative to the control run are observed in orbital cases A and C (Fig. 4B and D). During orbital case A, warming of up to 4 °C occurs over SE-Asia, central S-America and of ~3 °C over S-Africa. The largest difference in air temperature of all orbital runs is simulated to take place in orbital case C where temperatures rise up to 4 °C in the region north and south of 10–15°S (Fig. 4D). Very minor warming takes place within the drainage area of tropical Africa itself with cooling and warming of about 1 °C during orbital case A and C, and a fairly consistent warming of 1.5–2.0 °C during orbital case B. More variable and larger temperature changes are indicated for orbital case D, particularly north and south of 45°S and 45°N.

3.1.2. Sea level pressure

Different from temperature and precipitation data, simulated air pressure is not presented as deviation from the control run but in absolute values. Control run conditions simulate a pronounced latitudinal gradient in sea level pressure for the northern hemisphere (Fig. 5A). Low pressure is focussed to the ocean with values between 998 and 1005 hPa north of 50°N. Sea level pressure gradually increases to 1010–1015 hPa further south at 35–50°N to approach a band of high pressure of 1018–1026 hPa at 20–35°N. As for the high northern latitudes, highest pressure is located over the low-latitude ocean. Different from the mid and high northern latitudes, air pressure at sea level remains more homogeneous across the southern hemisphere with values between 1010 and 1015 hPa. This pattern is interrupted by a moderate high pressure systems located over the ocean at about 30°S and few local low pressure systems at 60°S with values down to 1005 hPa.

The general pattern does not change for the orbital runs but the magnitude of pressure differences varies according to precessional forcing (Fig. 5B–E). In orbital cases A and B, substantial weakening and strengthening around 30°N and 60°N is evident, as well as an expansion of the zones of highest and lowest pressure. As for the other parameters presented, the results imply the largest variation for tropical N-Africa during orbital runs A and C. It is important to note that the zone of relative high pressure at 30°S intensifies considerably during orbital case C (Fig. 5D). According to the data, a large high pressure cell established over the mid-latitude South Atlantic with 1023 hPa for case C compared to 1016 hPa for case A. Orbital cases C and D show a similar distribution and magnitude as indicated for the control run. As for the northward wind originating in southern Africa; the model does simulate weakest pressure gradients in the S-Atlantic in orbital case B (as shown in Fig. 5B–D). Fig. 6 displays latitudinal differences in air pressure for the region between 6–35°S and 32–42°W. The graph clearly illustrates that longitudinal pressure transects (mean data between 32–42°W) for all four orbital models indicate lower pressure south of the equator whereas they are higher at 35°S. The graph also illustrates that pressure gradients are lowest in “orba” and highest in “orbc”.

3.1.3. Surface winds

Global surface winds were analyzed to identify possible pathways for atmospheric water vapor transport from potential sources of moisture to the drainage area. The data from control run conditions for March indicate strong latitudinal zonation of surface winds (Fig. 7A). The polar and subpolar areas north and south of about 50–55° do not show winds surpassing 2 m/s. These weak winds are encompassed to lower latitudes by strong Westerlies that typically lie between the subtropical highs at 30°. The Westerlies are considerably stronger in the northern than in the southern hemisphere with wind speeds up to 11 m/s in the north compared to maximum speeds of about 5 m/s in the south. Between the subtropical highs and the equator, the NE-trade winds reach wind speeds of more than 11 m/s, whereas the SE-trades are absent over northern S-America and S-Africa. They vary around 4–6 m/s over stretches of open water of the proto-Indian Ocean and Pacific spanning a zone of 20° latitude and increase on the western coast of S-America and in the mid-latitude S-Atlantic to about 10 m/s and 5–8 m/s, respectively. It is important to note that these trade winds affect the equatorial African as southerly onshore winds.

With regard to the study area, the surface winds reveal an interesting pattern over the course of one precessional cycle. Compared to the control run, data for orbital case A suggest only minor variations (Fig.

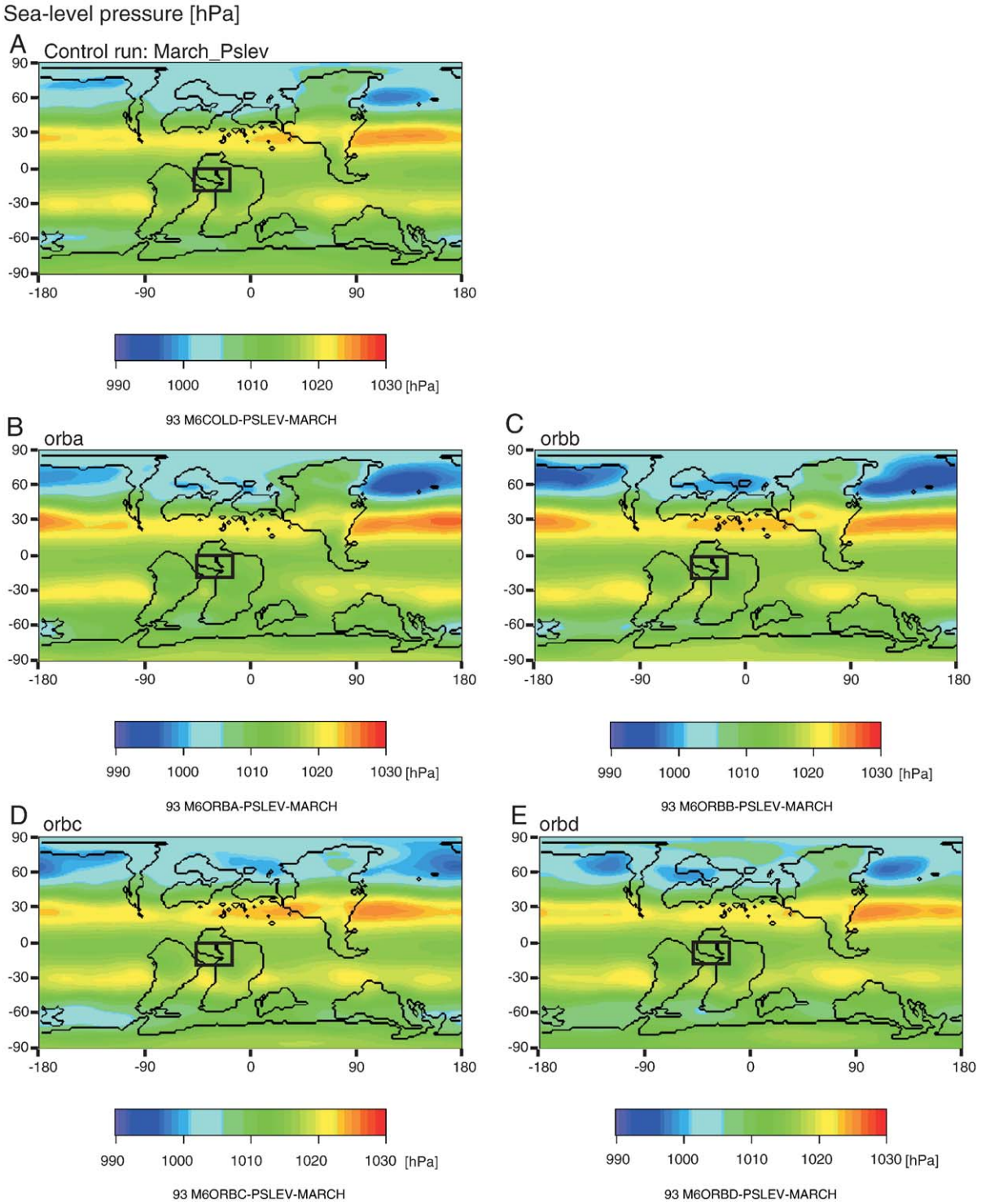

Fig. 5. Sea level pressure (hPa) for the month of March for the control run (A) and the orbital runs (B–E). The control run defines reference conditions. Figures B–E do show the results for global sea-level pressure according to variations in precessional forcing. The study area is highlighted by a black rectangle.

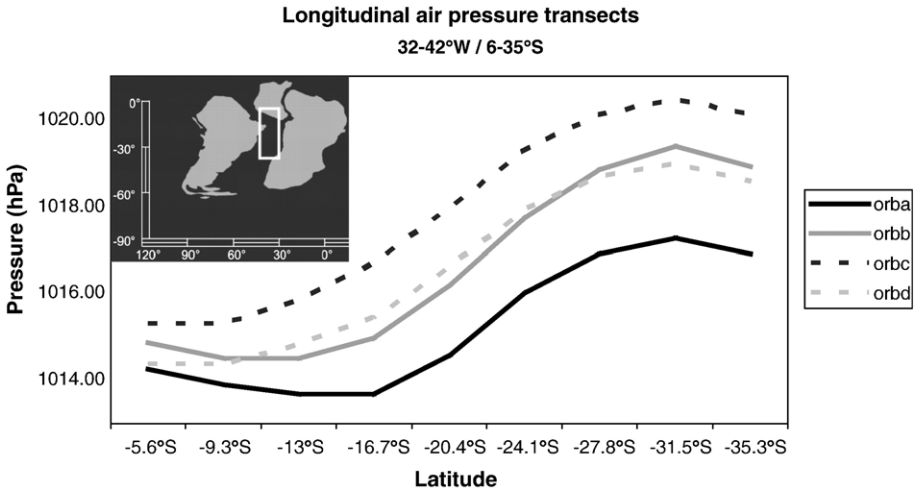

Fig. 6. Wind speed at sea level (m/s) for the control (A) and the orbital runs (B–E). All models show simulated wind speed and direction for the month of March. The area of interest is indicated by a white rectangle.

7B). The southerly winds originating in the central S-Atlantic do not vary in strength or direction, but provide an open connection between the mid-latitude S-Atlantic with winds of up to 8 m/s blowing across the S-Atlantic to tropical N-Africa. This wind system extends from about 25°S to 10°S and transported moisture from southern mid-latitudes to tropical Africa. Simultaneously, the northern hemisphere counterpart, the NE-trades decrease in strength by about 20% to less than 8 m/s supporting the expansion of southerly winds far onto the African continent. At 15°S over central S-Africa, a zone of northerly winds with moderate wind speeds of 2–4 m/s is present. This large-scale pattern slightly changes in orbital case B (Fig. 7C) when the wind system over central Africa disappears and the NE-trades further decrease in strength to 5–7 m/s. These conditions maintain the atmospheric connection between the central South Atlantic and tropical Africa open with wind speeds of up to 8 m/s. The magnitude of the competing wind systems change with the transition to orbital case C (Fig. 7D) as the NE-trades gradually increase in strength to approach up to 11 m/s. At the same time, winds over central Africa at 15°S decrease or breakdown supporting a strong attenuation of the southerly winds with maximum speeds of only 6 m/s and a change in direction, now blowing with an SSE component. Attenuation and deviation of wind directions from the mid-latitude S-Atlantic resulted in the closure or at least considerable weakening of the cross-latitudinal connection. Orbital case D (Fig. 7E) again represents a transitional phase with the NE-trades becoming slightly attenuated and the winds over the African interior remaining weak with hardly any direction to be assigned. The wind system of the central S-Atlantic is building up strength to establish a new cycle with an open connection between the mid-southern latitudes and tropical Africa.

3.1.4. Precipitation

Closely linked to air temperature, moisture transport and wind fields the global pattern reveals a distinct latitudinal distribution of precipitation (Fig. 8). The highest precipitation has been simulated for the equatorial region, which lies within the ITCZ. Values reach from 5 to 18 mm/day during control run conditions (Fig. 8A). Within the equatorial region, strongest precipitation occurs over the oceans, followed by large continental areas of northern S-America, SE-Asia and N-Africa. On the continents, values vary between 4 and 12 mm/day. At mid-latitudes, precipitation rapidly decreases to ~2–4 mm/day before it almost doubles to 4–8 mm/day at about 45°N and 45°S. Minimum values of 1–2 mm/day and below are modelled for the high latitudes and the continental interiors consistent with the distribution of global air temperature.

The simulations with varying orbital setups show evidence for dramatic effects of orbitally induced changes in precession on precipitation relative to the control run (Fig. 8B–E). As for air temperature, the most severe changes are simulated for orbital cases A and D. Strongest fluctuations in precipitation are indicated for the equatorial region, whereas latitudes north of 10°N and south of 25°S experienced only small changes compared to control run. N-Africa receives a considerable amount of excess precipitation

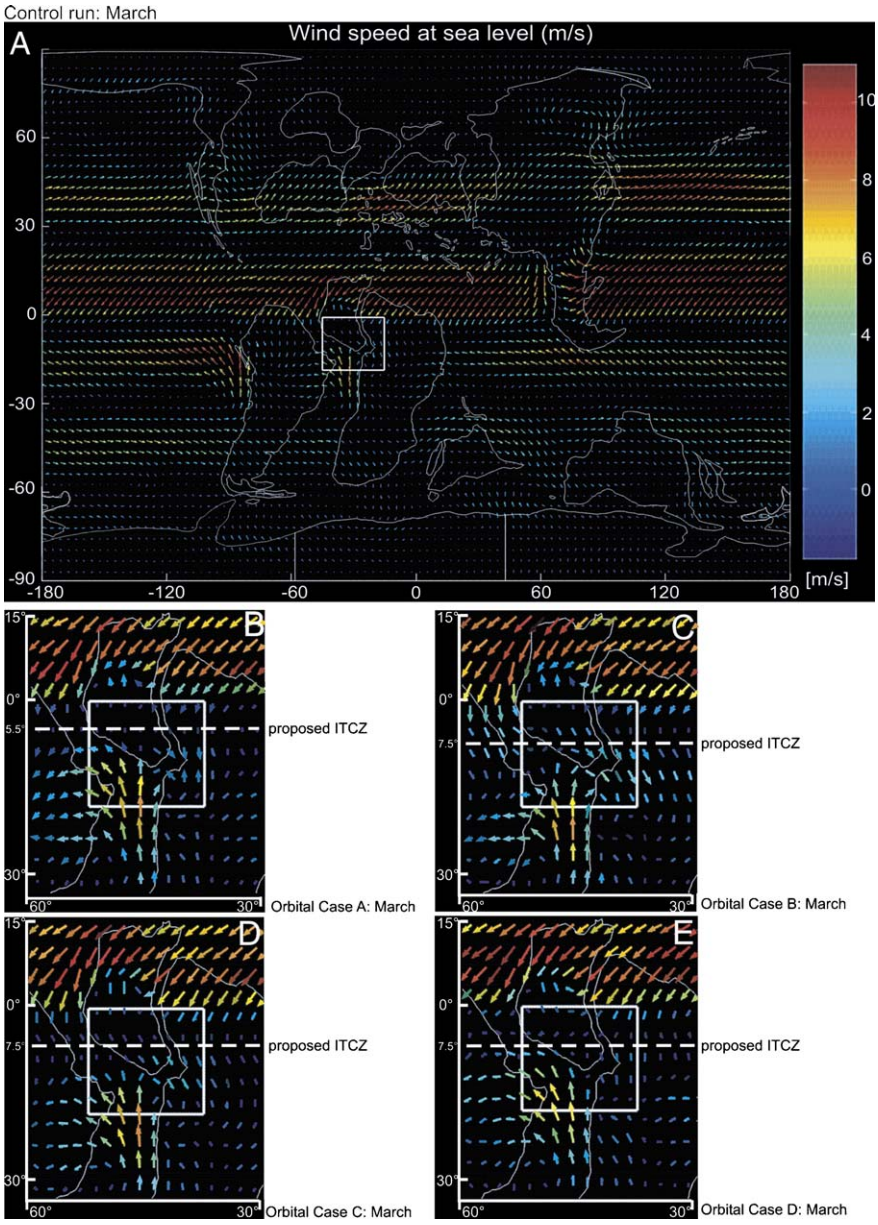

Fig. 7. (A) Solar insolation between 24.1°S and 54.5°S. Shown are the monthly average values for solar insolation at the top of the atmosphere. Values are in W/m^2 for the grid cells between 25–55°S and 180°W–180°E. (B) Precipitation (mm/day) between 1–19°S and 15–45°W. Data is shown for one complete precessional cycle. (C) Total river discharge (mm/day) between 1–19°S and 15–45°W. Data is shown for one complete precessional cycle.

during orbital case A with values higher than 2–4 mm/day when compared to the control run. Opposite to that, precipitation is lower by 3–5 mm/day during orbital case C relative to the control run providing a maximum difference between cases A and C on the order of 5–9 mm/day. Globally, the largest orbitally driven precipitation changes on the continents occur over parts of tropical N-Africa indicating severe changes in total river discharge to the Eastern Equatorial Atlantic and thus ODP Site 959. Orbital cases B and D represent intermediate patterns for the study area.

4. Discussion

The climate records from the eastern tropical Atlantic at ODP Site 959 off the Ivory Coast evidence long-term trends in African climate and systematic

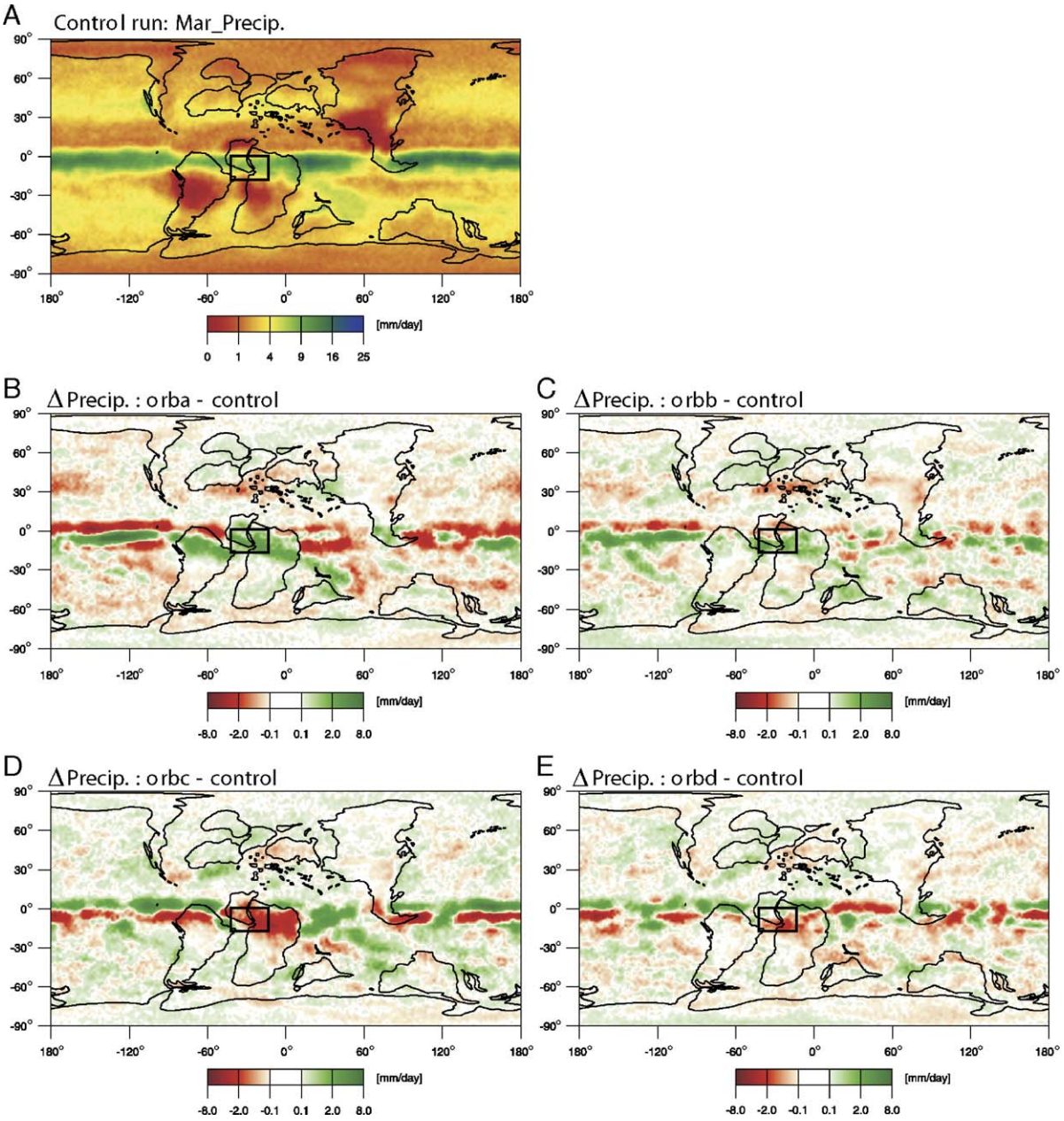

Fig. 8. A–E: Precipitation (mm/day) for the control (A) and the orbital runs (B–E). All models show simulated precipitation for the month of March. The area of interest is indicated by a white rectangle.

fluctuations in the degree of seasonal climate extremes as controlled by precessional forcing (Beckmann et al., 2005b). Most of all, they emphasize the role of distinct orbital configurations as primary drivers for the repetitive onset and termination of marine black shale sedimentation (e.g., Hofmann et al., 2003; Wagner et al., 2004). The transformation of orbital forcing down to marine carbon burial involves a succession of processes and feedback mechanisms that determine climate and the hydrologic cycle. The process of signal formation at the ocean floor starts at the top of the atmosphere with solar insolation. Insolation is the key driver for evaporation, atmospheric transport of moisture, precipitation, surface and subsurface runoff, and ultimately total river discharge. As total river discharge is assumed to be the most important control mechanism for organic carbon accumulation on Site 959, we address all subcompart-

ments, from the top of the atmosphere to Earth's surface and further to the sea floor.

Model data for Cretaceous annual insolation (W/m^2) for a latitudinal band spanning 180°W–180°E and 24.1–54.5°S on a monthly base propose high energy yields during boreal winter/austral summer and vice versa with average values from 300–500 W/m^2 during September to March and 130–300 W/m^2 during April

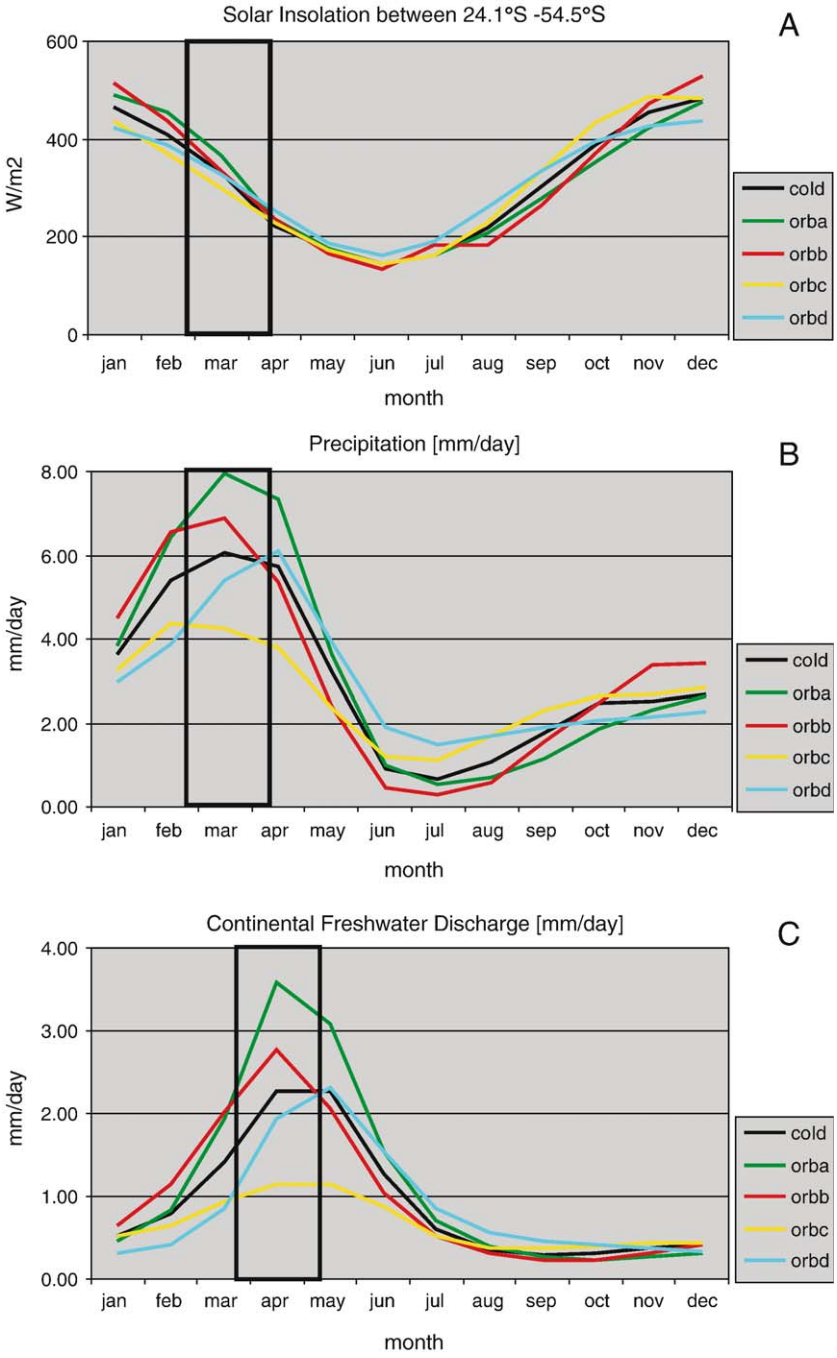

Fig. 9. A–C: (A) - Solar insolation between 24.1°S and 54.5°S. Shown are the monthly average values for zonal solar insolation at the top of the atmosphere. Values are in W/m^2 for the grid cells between 25–55°S and 180°W–180°E. (B) - Precipitation (mm/day) between 1–19°S and 15–45°W. Data are shown for one complete precessional cycle. (C) - Total river discharge (mm/day) between 1–19°S and 15–45°W. Data are shown for one complete precessional cycle. All values for precipitation and continental freshwater discharge are data for the continental part of the study area only.

to August (Fig. 9A). The described latitudinal band was chosen because of the observed high sensitivity in this region which results in a global high pressure zone located between 24°S and 54°S. This zone has been simulated for all four models. Variations across the five models are largest from August through March with maximum values in December and January, but almost identical during summer months May to July. For February and March, the months when signal formation primarily occurred at Site 959, seasonal insolation is highest during orbital case A (453 to 367 W/m^2 from February to March) and lowest in orbital case C (371 to 299 W/m^2 from February to March) with an offset of only 14 W/m^2, from 86 W/m^2 in A to 72 W/m^2 in C. The value for Cretaceous global mean annual insolation is simulated to be ~293 W/m^2 for all five models. To put these data from the Cretaceous into a modern context, we compare them to global data representing the largest variability during the past 100 ka. Due to changes in the precession of the equinoxes, mid-latitude northern hemisphere insolation values at summer solstice have varied by about 8% around the mean (~40 W/m^2, Imbrie et al., 1993) over the last 100 ka. For comparison, this value is large compared to a climatic forcing of 4 W/m^2 as simulated for a doubling of atmospheric CO_2 concentrations under modern boundary conditions (Cess and Vulis, 1989). Due to a low eccentricity of 0.0167, the present day difference in insolation between perihelion and aphelion is ~6.4 W/m^2 (Loutre and Berger, 2000), whereas a highly elliptical orbit (0.05), as used in our simulations, produces a change in the amount of insolation received at perihelion on the order of 20% to 30% greater than at aphelion (Milankovitch, 1941), consequently resulting in a substantially different climate from what we experience today. Due to the high eccentricity of 0.05, all these "modern world" data are smaller than the Cretaceous ones illustrating that orbital forcing of climate is critical during greenhouse conditions. Additionally, we assume that internal feedback loops within the atmosphere, probably involving enhanced cross-latitudinal latent heat transfer combined with increased water vapor content near saturation are responsible for the sensitivity of a greenhouse climate.

Different from Cretaceous insolation and offset in time is the annual record of simulated precipitation (Fig. 9B). Precipitation acts as a transport mechanism, linking the top of the atmosphere with processes at the Earth's surface and thus may be expected to mirror or at least correlate to solar insolation on various scales, within the hemispheres and probably regionally. Monthly distribution of precipitation during the Cretaceous is simulated to be highest in spring (March and April) when isolation was half way on its gradual decrease in energy supply. This observation is independent from the orbital model despite large offsets between individual cases during maximum spring precipitation. Different from the timing of insolation and precipitation maxima, summer insolation is at minimum coincident with lowest precipitation. Present day precipitation data from the tropical African cities of Lome (Togo) and Ibadan (Nigeria) show an offset of peak precipitation of 3–4 months (http://sandmc.pwv.gov.za/safari2000/nasa/rain/cntrlist.asp) relative to Cretaceous simulations. This offset may be explained by the combination of paleogeography, atmospheric CO_2 and heat transport mechanisms. The mid-Cretaceous study area was set between 1°S and 19°S instead of 6–8°N for the present day cities of Lome and Ibadan. Data from these two locations do not represent the modern climate situation at full range considering that modern precipitation inland central Africa (Sahel/Sahara) range from 8 to 0 mm/day. Therefore, measurements from two stations are not representative, neither in amplitude nor timing of peak precipitation. Unfortunately, no data for a region comparable to the Cretaceous study area was available. Atmosphere CO_2 likely acts as another parameter to explain the observed time offset in maximum precipitation. CO_2 content for the Cretaceous simulations was set to 1881.6 ppm supporting a global greenhouse climate. Our current knowledge on the general mechanisms, feedback loops and fluxes within the system during these conditions are still not satisfactory. Because CO_2 affects the hydrologic cycle through temperature, climate is a pas de deux between CO_2 and H_2O (Pierrehumbert, 2002).

Finally, the aspect of heat transport mechanism has to be considered. A greenhouse climate is dominated by a meridional temperature gradient ΔT that describes heat transport carried by the atmosphere and ocean. During Cretaceous greenhouse conditions, it was probably maintained by enhanced fluxes of latent heat (Pierrehumbert, 2002). Allen and Ingram (2002) further emphasize that tropospheric specific humidity's rise parallel with surface warming and more-or-less unchanged relative humidity. The distribution of moisture in the troposphere, being the part of the atmosphere that is strongly coupled to the surface, is complex but that there is one strong control which is: moisture condenses out of supersaturated air. Furthermore, the distribution of relative humidity is thought to remain constant under climate change, whereas the Clausius–Clapeyron relation implies that specific humidity does increase roughly exponentially

with temperature. But numeric simulations of climate warming have shown that relative humidity seems to change little, at least at low latitudes (Ingram, 2002), whereas rising specific humidity levels at the surface have been observed over parts of the northern hemisphere (New et al., 2000).

And fourthly, another plausible mechanism to shift peak precipitation lies within the setup of the various models. Compared to a present day eccentricity of 0.0167 (close to circular), the chosen value for the Late Cretaceous simulations is 0.05 (close to highest eccentricity of 0.075). This was kept constant throughout the suite of models. As a result of a highly eccentric orbit, the seasons are more pronounced which in turn amplifies their climatic signal when compared to, e.g., the present day. By increasing seasonality, above all, we enhance the forcing during orbital case A (spring equinox at perihelion), followed by the two intermediate cases B and D where the equinoxes coincide neither with aphelion or perihelion. The lowest spring forcing occurs when the spring equinox coincides with aphelion.

To explain the shift in peak precipitation from March and April during our simulations and from May to July during the present day, one or more of the proposed ideas apply most presumably the set value for eccentricity.

The simulated precipitation data suggest an overall sinusoidal shape over the course of one cycle, with the highest precipitation being simulated for orbital case A with 3.28 mm/day mean annual and the lowest value of 2.70 mm/day mean annual for orbital case C. Compared to the present day, simulated results from a GENESIS simulation with modern day boundary conditions calculated 1.76 mm/day for the same region as the study area. The largest variation occurs during spring configuration (March and April) when precipitation is enhanced by 31% in orbital case A and reduced by 30% in orbital case C relative to control conditions ("cold" model).

The next parameter following along the hydrological cycle is freshwater runoff, which is determined by precipitation and (evapo-) transpiration. Factors controlling runoff and considered in GENESIS 2.0 include the rate of precipitation, saturation state of the soil, geology of the substrate, slope and vegetation, and likely not relevant for the Cretaceous the rate of melting of accumulated snow. In climate models, runoff occurs when the precipitation rate (or the snowmelt rate) exceeds the infiltration rate into the soil. Vegetation serves to deplete soil moisture between rainfall events and acts as one agent that separates surface from subsurface runoff. For the purpose of this study, we do not distinguish between the two associated processes but consider total freshwater discharge only.

As documented by Beckmann et al. (2005b), total discharge reveals a pronounced wet season from March to June with total discharge and a dry season from July to February (Fig. 9C). The maximum in total runoff is delayed relative to that in precipitation by 1 or 2 months. A river routing scheme is not available yet for GENESIS; however, it is not critical for this study to specifically know where the local runoff in the chosen rectangle emerged on the mid-Cretaceous African coast. The application of a river routing treatment would delay the seasonal peak of discharge by several weeks, at least while the fresh water is traveling to the coast. For the modern Amazon basin, for example, the delay is up to several months with highest precipitation in January followed by maximum fresh water discharge in May (Vörösmarty et al., 1996; Coe, 2000). Since the Mid-Cretaceous river system in tropical N-Africa probably was much shorter than the present day Amazon one, it appears reasonable to expect a delay time on the order of a few weeks. The modeling data presented support this time relationship and thus are consistent with theoretical considerations and modern observations.

4.1. Linking compartments of the hydrological cycle during the Late Cretaceous greenhouse—from local geological record-based models to global observations

The results from global modeling and simulated seasonal variability of main climate parameters explain the intrinsic linkage between precessional forcing with the various compartments of the hydrological cycle during greenhouse conditions. They also support a substantial interaction between the hydrological cycle and atmospheric circulation on regional and hemispheric scales during times of global warmth, as has been inferred from climate records of ODP Site 959 in the eastern tropical Atlantic (Beckmann et al., 2005a). Despite this general agreement with tropical geological records there is one contradiction, i.e., the possibility that the tropics act as a driver of global climate, at least during Cretaceous greenhouse conditions. The climate simulations presented challenge or at least qualify that fundamental conclusion. Instead, they provide evidence that the regional and cross-latitudinal evolution of air pressure and wind fields directly linked tropical Africa with the mid-southern latitudes. The establishment of a cross-latitudinal connection between mid-southern latitudes and tropical Africa, however, was not permanent throughout the precessional cycle but confined to the

specific orbital configurations simulated in orbital cases A and B. These represent orbital boundary conditions, which put the northern spring equinox and northern winter solstice at perihelion equivalent to the modern spring and summer seasons. Taking into account that the highest discharge from tropical Africa and slightly delayed, enhanced organic carbon burial in the tropical Atlantic only occurred during orbital case A (Beckmann et al., 2005b), we propose that Coniacian–Santonian tropical marine black shale formation was ultimately triggered by climate change in mid-southern latitudes. The mechanism connecting the trigger source area to the response area is suggested to be the temporal establishment of an atmospheric connection that imported humidity from the south to the response area in the north. What remains difficult to identify is the source area for excess humidity that is finally precipitated in tropical Africa, especially during the even more balanced climatic state of the spring (orbital case A) equinox. The cross-latitudinal atmospheric connection suggests a southern mid-latitude source. Precessionally driven changes in insolation between 25°S and 55°S, however, do not vary by more than 11% during March and April when compared to control run conditions. These minor changes are not sufficient to explain spring tropical African precipitation. First-order approximations off maximum humidity generated in the south and excess precipitation in tropical Africa reveal a misbalance of ~2 mm/day when compared to the reference model (control run). This misbalance may be expected to some extend and have a number of reasons. Most of all, the source for excess moisture was not in the atmospheric layer a few meters above the Earth's surface, as simulated in this study but within the boundary layer (Ross et al., 2001) at higher atmospheric levels and/or lower-tropospheric to mid-tropospheric levels (Zhai and Eskridge, 1997). As an alternative or supplement, we speculate that excess humidity in the tropics may have not been delivered from one specific region but was rather provided as water vapour of the greenhouse atmosphere from the northern and southern hemisphere mid-latitudes—a theory that needs to be further tested in the future. Finally, we cannot rule out that internal feedbacks loops related to non-linear translations of the insolation signal to the climate system have amplified or attenuated the atmospheric signal on its way to the tropical response area.

5. Conclusion

Modifying the analytical setup of GENESIS 2.0 to simulate and quantify the individual effect of precessional forcing by changing only the precession of the equinoxes, whereas eccentricity and obliquity are fixed to allow for maximum seasonality. On short orbital timescales, this study provides new insights to the internal dynamics of climate, the different compartments of the hydrological cycle and finally the sedimentary response within the oceanic realm during Cretaceous greenhouse conditions. Modelling the early Late Cretaceous (93 Ma, earliest Turonian) climate does not support a substantial latitudinal movement of the ITCZ along the precessional cycle as has been postulated by the climate record-based geological model from ODP Site 959 (Hofmann et al., 2003). Instead, the modeling results propose that the cross-latitudinal evolution of air pressure and wind fields linked tropical Africa to the mid-southern latitudes, at least during modern spring and summer orbital configurations. This cross-latitudinal atmospheric connection has not been recognized before and raises the idea that the role of the tropics as an important driver of Cretaceous climate is reduced compared to the modern day. Following the new results, we conclude that tropical Atlantic black shale formation in the Late Cretaceous was ultimately triggered by climate change in mid-southern latitudes although indirectly transmitted through precipitation and runoff from tropical N-Africa. The mechanism connecting the trigger source area to the response area was the temporal establishment of an atmospheric connection that imported humidity from the south to the response area in the north. Confining the mid-latitude S-Atlantic region as a prime source area for moisture for tropical N-Africa remains difficult, likely because excess moisture was generated and transported at higher atmospheric and/or tropospheric levels than analyzed for this study. We also invoke that excess humidity was provided as water vapour from the northern and southern hemisphere mid-latitude atmosphere. Despite uncertainties about the source area of moisture, the simulation of seasonal insolation supports the conclusion that forcing of climate during Cretaceous greenhouse conditions requested about similar or higher variations of solar energy as calculated for the present day and the past 100 ka. Obviously, a greenhouse climate scenario is not more sensitive as the present day climate system. As a working hypothesis that can be tested in the near future, we speculate that the mid-latitudes represent the "ultimate" region of climate signal formation during times of extreme global warmth. If the working hypothesis is supported by other investigations, we suspect that the progressive warming of the atmosphere in the future may result in a gradual migration of the prime climate trigger area towards mid latitudes.

Acknowledgements

We are indebted to David Pollard who helped us gain detailed knowledge of GENESIS. We also thank Mithun Aiyswaryan for generating some of the data. This work was supported by the DFG grant HA 2891/3-2, Wa1036/7, and the Gottfried Wilhelm Leibniz Award Leibniz 2002.

We also thank W. Chr. Dullo for his thoughtful comments on a former version of this manuscript.

We finally thank an anonymous reviewer and Karen Bice for critical and instructive reviews that essentially helped to improve the focus and quality of this manuscript.

References

Allen, M.R., Ingram, W.I., 2002. Constraints on future changes in climate and the hydrological cycle. Nature 419, 224–232.

Balukhovsky, A.N., Floegel, S., Hay, W.W., Migdisov, A., Wold, C.N., 2004. A paleogeograhic map for the Lower Turonian. EarthRef Digital Archive: http://earthref.org/cgi-bin/erda.cgi?n=220.

Beckmann, B., Hofmann, P., Wagner, T., 2005a. Linking Coniacian-Santonian (OAE3) black shale formation to African climate variability: a reference section from the eastern tropical Atlantic at orbital time scales (ODP Site 959, off Ivory Coast/Ghana). In: Pradier, B., Harris, N. (Eds.), Source Rock Development: Bioproductivity, Organic Preservation, or Sedimentation Rate? SEPM Special Publication, vol. 82, pp. 125–143.

Beckmann, B., Flögel, S., Hofmann, P., Schulz, M., Wagner, T., 2005b. Orbital forcing of cretaceous river discharge in tropical Africa and ocean response. Nature 437, 241–244.

Berger, A.L., 1978. Long term variations of daily insolation and quaternary climatic changes. Journal of the Atmospheric Sciences 35 (12), 2362–2367.

Berner, R.A., 1994. GEOCARB II: a revised model of atmospheric CO_2 over Phanerozoic time. American Journal of Science 294, 56–91.

Cerling, T.E., 1991. Carbon dioxide in the atmosphere: evidence from Cenozoic and Mesozoic paleosols. American Journal of Science 291, 377–400.

Cess, R.D., Vulis, I.L., 1989. Inferring surface solar absorption from broadband satellite measurements. Journal of Climate 2, 974–985.

Coe, M.T., 2000. Modeling terrestrial hydrologic systems at the continental scale: testing the accuracy of an atmospheric GCM. Journal of Climate 13, 686–704.

Covey, C., Thompson, S.L., 1989. Testing the effects of ocean heat transport on climate. Paleogeography, Paleoclimatology, Paleoecology 75, 331–341.

Crowley, T.J., Baum, S.K., Kim, K.-Y., 1993. General circulation model sensitivity experiments with pole-centered supercontinents. Journal of Geophysical Research 98, 8793–8800.

DeConto, R.M., Brady, E.C., Bergengren, J., Hay, W.W., 2000. Late Cretaceous climate, vegetation, and ocean interactions. In: Huber, B.T., MacLeod, K.G., Wing, S.L. (Eds.), Warm Climates in Earth History. Cambridge University Press, pp. 275–296.

Dorman, J.L., Sellers, P.J., 1989. A global climatology of albedo, roughness length and stomatal resistance for atmospheric general circulation models as represented by the Simple Biosphere model (SiB). Journal of Applied Meteorology 28, 833–855.

Floegel, S., Hay, W.W., DeConto, R.M., Balukhovsky, A.N., 2005. Formation of sedimentary bedding couplets in the Western Interior Seaway of North America—implications from Climate System Modeling. Palaeogeography, Palaeoclimatology, Palaeoecology 218, 125–143.

Gough, D.O., 1981. Solar interior structure and luminosity variations. Solar Physics 74, 21–34.

Hofmann, P., Beckmann, B., Wagner, T., 2003. A millennial- to centennial-scale record of African climate variability and organic carbon accumulation in the Coniacian–Santonian eastern tropical Atlantic (ODP Site 959, off Ivory Coast/Ghana). Geology 31 (2), 135–138.

Huber, B.T., 1998. Tropical paradise at the Cretaceous poles? Science 282, 2199–2200.

Imbrie, J., Berger, A., Boyle, E., Clemens, S., Duffy, A., Howard, W., Kukla, G., Kutzbach, J., Martinson, D., McIntyre, A., Mix, A., Molfino, B., Morley, J., Peterson, L., Pisias, N., Prell, W., Raymo, M., Shackleton, N., Toggweiler, J., 1993. On the structure and origin of major glaciation cycles: 2. The 100,000-year cycle. Paleoceanography 8, 699–735.

Ingram, W.J., 2002. On the robustness of the water vapor feedback: GCM vertical resolution formulation. Journal of Climate 15, 917–921.

Loutre, M.F., Berger, A., 2000. Future climatic changes: are we entering an exceptionally long interglacial? Climatic Change 46 (1–2), 61–90.

Milankovitch, M.M., 1941. Kanon der Erdbestrahlung. Beograd. Königlich Serbische Akademie. 484 pp.

New, M., Hulme, M., Jones, P., 2000. Representing twentieth-century space–time climate variability: Part II. Development of 1901–1996 monthly grids of terrestrial surface climate. Journal of Climate 13, 2217–2238.

Pierrehumbert, R.T., 2002. The hydrological cycle in deep-time climate problems. Nature 419, 191–198.

Pletsch, T., et al., 2001. Cretaceous opening history of the Equatorial Atlantic Gateway: the view from the West African continental margin (ODP Leg 159). Journal of South American Earth Sciences 14, 147–174.

Pollard, D., Thompson, S.L., 1995. Use of a land-surface-transfer scheme (LSX) in a global climate model (GENESIS): the response to doubling stomatal resistance. Global and Planetary Change (MECCA special issue) 10, 129–161.

Poulsen, C.J., Barron, E.J., Arthur, M.A., Peterson, W.H., 2001. Response of the mid-Cretaceous global oceanic circulation to tectonic and CO_2 forcings. Paleoceanography 16, 576–592.

Ronov, A., Khain, V., Seslavinsky, K., 1984. Atlas of Lithological-Paleogeographical Maps of the World, Late Precambrian and Paleozoic of Continents. U.S.S.R. Academy of Sciences, Leningrad. 70 pp.

Ronov, A.B., Khain, V.E., Balukhovsky, A.N., 1989. Atlas of Lithological-Paleogeographical Maps of the World: Mesozoic and Cenozoic of Continents and Oceans. In: Barsukov, V.L., Laviorov, N.P. (Eds.), Editorial Publishing Group VNIIZarubezh-geologia, Moscow, p. 79.

Ross, R.J., Elliott, W.P., Seidel, D.J., 2001. Lower-tropospheric humidity–temperature relationships in radiosonde observations and atmospheric general circulation models. Journal of Hydrometeorology 3, 26–38.

Shea, D.J., 1986. 1950–1979 Surface Air Temperature, Precipitation, Sea-Level Pressure, and Sea-Surface Temperature (45S-90N). NCAR/TN-269+STR Climatological Atlas., NCAR, Boulder, CO. 35 pp plus 158 figures and 10 microfiche.

Sloan, L.C., Morrill, C., 1998. Orbital forcing and Eocene continental temperatures. Palaeogeography, Palaeoclimatology, Palaeoecology 144, 21–35.

Thompson, S.L., Pollard, D., 1995. A global climate model (GENESIS) with a land-surface-transfer scheme (LSX). Part 1: present-day climate. Journal of Climate 8, 732–761.

Thompson, S.L., Pollard, D., 1997. Greenland and Antarctic mass balances for present and doubled CO_2 from the GENESIS version-2 global climate model. Journal of Climate 10, 871–900.

Voigt, S., Gale, A.S., Flögel, S., 2004. Midlatitude shelf seas in the Cenomanian–Turonian greenhouse world: temperature evolution and North Atlantic circulation. Paleoceanography 19, 1–17 (PA4020).

Vörösmarty, C.J., Willmott, B.J., Choudhury, A.L., Schloss, T.K., Stearns, S.M., Robeson, T.J., Dorman, T.J., 1996. Analyzing the discharge regime of a large tropical river through remote sensing, ground-based climatic data, and modeling. Water Resources Research 32, 3137–3150.

Wagner, T., 2002. Late Cretaceous to Early Quaternary organic sedimentation in the Eastern Equatorial Atlantic. Palaeogeography, Palaeoclimatology, Palaeoecology 179, 113–147.

Wagner, T., Pletsch, T., 1999. Tectono-sedimentary controls on Cretaceous black shale deposition along the opening Equatorial Atlantic Gateway (ODP Leg 159). In: Cameron, N., Bate, R., Clure, V. (Eds.), The Oil and Gas Habitat of the South Atlantic. The Geological Society of London, London, pp. 241–265.

Wagner, T., Sinninghe Damsté, J., Beckmann, B., Hofmann, P., 2004. Euxinia and primary production in Upper Cretaceous Eastern Equatorial Atlantic surface waters fostered orbital-driven formation of marine black shales. Paleoceanography 19, A3009. doi:10.1029/2003PA000898.

Wilson, P.A., Norris, R.D., 2001. Warm tropical ocean surface and global anoxia during the mid-Cretaceous period. Nature 412, 425–429.

Zhai, P.M., Eskridge, R.E., 1997. Atmospheric water vapor over China. Journal of Climate 10, 2643–2652.